

## Probing photodegradation beneath the surface: a depth profiling study of UV-degraded polymeric coatings with microchemical imaging and nanoindentation

Xiaohong Gu, Chris A. Michaels, Peter L. Drzal,  
Joan Jasmin, David Martin, Tinh Nguyen, Jonathan W. Martin

© FSCT and OCCA 2007

**Abstract** Photodegradation of polymer coatings generally involves photooxidation, resulting in the formation of oxidized products, chain scission, and crosslinking. On severe exposure to ultraviolet (UV) light in the presence of air, chemical degradation transforms into substantial changes in the physical and mechanical properties, leading to failures of the coatings. Systematic research by NIST on service life prediction of polymeric coatings indicates that the degradation of polymer coatings starts from the sub-micrometer degradation-susceptible regions at the surface and then grows in width and depth. Additionally, due to the oxygen diffusion effect and the attenuation of the UV light passing through the polymer, the degradation can be spatially heterogeneous. In this study, the changes with depth of the mechanical and chemical properties of a UV-exposed epoxy/polyurethane system were measured by nanoindentation and Fourier transform infrared spectroscopy (FTIR) microscopy using cross-sectioned specimens. Multilayers of epoxy/polyurethane samples were prepared by a draw-down technique. After curing, samples were exposed to the outdoors in Gaithersburg, MD, for four months. Cross-sectioned slices of the exposed and unexposed samples,

approximately 500 nm thick as-prepared by microtoming, were used for micro-FTIR imaging. Samples for nanoindentation were prepared by embedding the epoxy/polyurethane multilayers (both exposed and unexposed) in a molding compound, followed by microtoming and polishing the embedded films in the thickness direction. Micro-FTIR images clearly show that, for the outdoor exposed samples, substantial amounts of oxidation products are distributed in the 60  $\mu\text{m}$  deep region from the surface to the epoxy bulk, decreasing in the center of epoxy region and increasing again toward the epoxy/urethane interface. Nanoindentation results also show that the modulus significantly increases in the first 60  $\mu\text{m}$  region after UV degradation, and then decreases gradually with depth until a value slightly higher than the modulus of the undegraded epoxy is reached. The modulus rises again in the region near the epoxy/urethane interface. These similarities in the depth profiles of the properties indicate the linkage between the chemical degradation and the mechanical degradation. The study clearly shows that the spatial distribution of chemical species and mechanical properties is heterogeneous in the thickness direction for polymer coatings after UV degradation. It also demonstrates that cross-sectional analysis using nanoindentation and micro-FTIR imaging techniques is a useful method to characterize the mechanical and chemical depth profiles of polymer coating degradation.

---

Presented at the 2006 FutureCoat! Conference sponsored by the Federation of Societies for Coatings Technology, in New Orleans, LA, on November 1–3, 2006. Awarded 1st place in the 2006 John A. Gordon Best Paper competition.

---

X. Gu (✉), C. A. Michaels, P. L. Drzal,  
J. Jasmin, D. Martin, T. Nguyen, J. W. Martin  
Building and Fire Research Laboratory, National Institute  
of Standards and Technology, Gaithersburg, MD 20899,  
USA  
e-mail: xiaohong.gu@nist.gov

*Present Address:*

P. L. Drzal  
PPG Industries, Inc., Allison Park, PA 15101, USA

**Keywords** Nanoindentation, FTIR-microscopy, Photodegradation, Epoxy resins, Polyurethanes, Mechanical properties, Physical properties, Weatherability

### Introduction

Polymeric materials are generally susceptible to oxidative degradation when exposed to ultraviolet (UV)

irradiation or heat in the presence of oxygen due to the formation of free radicals and other reactive intermediates.<sup>1</sup> The chemical modification of polymers resulting from photooxidation would lead to changes in physical and mechanical properties, such as molecular mass,<sup>2</sup> crosslinking density,<sup>3,4</sup> glass transition temperature ( $T_g$ ),<sup>3,4</sup> modulus and hardness,<sup>5,6</sup> roughness and gloss.<sup>7,8</sup> Extensive studies by NIST<sup>6,9–12</sup> on service life prediction of polymeric materials from nanoscale to macroscale via atomic force microscopy, confocal microscopy, nanoindentation and spectroscopy, indicate that degradation of polymeric materials initiates at sub-micrometer degradation-susceptible regions on the surface, and then the degraded regions expand, deepen, and aggregate with longer exposures. The photodegradation mode of polymeric materials appears as a heterogeneous process rather than an ablation.<sup>13</sup> Additionally, in the case of photooxidation, because of the oxygen diffusion effect and the attenuation of the UV light passing through the polymer,<sup>14</sup> the degradation could be spatially heterogeneous, both laterally along the sample surface and along the thickness direction perpendicular to the surface. This spatial heterogeneity implies that a thorough characterization of photodegradation is challenging, and the conventional techniques for bulk property characterization such as regular Fourier transform infrared spectroscopy (FTIR), and dynamic mechanical analysis, may not reveal the detailed property changes resulting from UV irradiation. Therefore, it is necessary to develop depth-profiling techniques to characterize the spatial distribution of the chemical species resulting from photodegradation and the variation in physical or mechanical properties along the direction normal to the sample surface.

Attenuated total reflectance FTIR (ATR-FTIR) and photoacoustic spectroscopy FTIR (PAS-FTIR) are two common techniques used to follow chemical changes during polymer degradation, mainly due to their non-destructive sampling and the ability to provide chemical structural information at different depths of the sample.<sup>15–17</sup> The spatial effect in the photodegradation of poly (acrylonitrile-butadiene-styrene) has been studied by ATR-FTIR using microtomed sections.<sup>15</sup> It was found that the spatial distribution of degradation products is heterogeneous; significant amounts of photoproducts were detected only in the top irradiated layer of approximately 50  $\mu\text{m}$  depth. However, ATR-FTIR is more suitable for the investigation of surfaces and of layers close to the surface than for the bulk. The analyzed depth is wavelength-dependent and ranges from 0.5 to 2.8  $\mu\text{m}$  (3600–600  $\text{cm}^{-1}$ ) for ATR equipped with a germanium crystal.<sup>16</sup> By changing the modulation frequency of the IR radiation, i.e., the mirror velocity of the FTIR spectrometer, photoacoustic spectroscopy (PAS) can be employed to study layers at various depths below the surface of a sample. This technique therefore allows depth-profile analysis of heterogeneous polymers.<sup>17,18</sup> Quantitative spectroscopy with this technique can be relatively difficult. Unlike other vibrational

techniques such as ATR-FTIR, which depend largely on the optical properties of the material, a photoacoustic signal is also coupled to the thermal properties of the sample, and particularly, is a function of the modulation frequency of the incident light beam.<sup>17</sup> While the frequency dependence can be eliminated by the use of step scan interferometric detection,<sup>18,19</sup> thermal heterogeneity of polymeric films and coatings, resulting from either processing or degradation, can pose significant problems. Therefore, theoretical thermal models are generally needed for estimating the penetration depth in order to use step-scan PAS-FTIR to depth profile heterogeneous polymers.

Micro-FTIR is an effective technique to characterize the depth profiles of degradation through cross-sectional analysis of microtomed layers. Gardette et al.<sup>20–24</sup> have used micro-FTIR to study the photodegradation of polymers such as polystyrene, polycarbonates, and epoxy. A spatial heterogeneous distribution of the oxidation photoproducts has been observed for all these systems. By comparing micro-FTIR with PAS-FTIR, Gonon et al.<sup>17,24</sup> found good agreement between the two methods in the region from 11 to 22  $\mu\text{m}$  where the analyzed layers overlapped. PAS was found to be more suitable to determine the superficial extent of degradation, whereas the micro-FTIR appeared more adapted to depth profiling the bulk properties. Since the sample is prepared as microtome slices perpendicular to the surface, the drawback of this technique (i.e., micro-IR) is that the surface could be partially damaged by the microtome. The size of the regions that can be studied in this way can be as small as a few microns.

AFM nanoindentation and instrumented indentation testing (IIT) are two advanced, newly developed techniques for depth profiling the mechanical properties of photodegraded polymers. Mailhot et al.<sup>14,16</sup> have recently used AFM nanoindentation to study the heterogeneity of the mechanical properties of photooxidized epoxy resins. An increase or a decrease in the stiffness was found near the surfaces of different epoxy systems, which was attributed to different degradation mechanisms, e.g., crosslinking or scission reaction. However, instrumental uncertainties can affect AFM indentation measurement. The typical instrumental uncertainties include the uncertainties in optical lever detection systems, piezo nonlinearities, lateral motion of the probe tip due to bending of the cantilever, cantilever stiffness uncertainty, and contact area determination.<sup>25</sup> These errors will then propagate through the calculations of tip deflection and indentation displacement, affecting the determination of nanomechanical properties of the sample.

Instrumented indentation testing (IIT) or nanoindentation is increasingly being used to probe the mechanical properties of materials. Although originally developed for indentation of metals and ceramics, nanoindentation has been successfully demonstrated as a polymeric material characterization tool<sup>26–29</sup> through the use of depth sensing indentation (DSI). DSI

continuously measures the stiffness of the indenter/sample interaction as the indenter travels into the material. By modeling the instrument as a damped harmonic oscillator, a continuous value of stiffness is calculated throughout the loading curve. With the area function of the indenter tip determined from calibration procedures in a known standard, equation (1) can be used to calculate the effective elastic modulus ( $E_{\text{effective}}$ ) for any indenter tip that creates a circular contact. The sample modulus ( $E_{\text{sample}}$ ) can then be calculated from equation (2) with knowledge of the sample Poisson's ratio ( $\nu_{\text{sample}}$ ) and the indenter elastic modulus ( $E_{\text{indenter}}$ ) and indenter Poisson's ratio ( $\nu_{\text{indenter}}$ ).

$$E_{\text{effective}} = \frac{\sqrt{\pi} S}{2 \sqrt{A}} \quad (1)$$

$$\frac{1}{E_{\text{effective}}} = \frac{(1 - \nu_{\text{sample}}^2)}{E_{\text{sample}}} + \frac{(1 - \nu_{\text{indenter}}^2)}{E_{\text{indenter}}} \quad (2)$$

Care must be taken when conducting IIT testing on polymeric materials since the inherent viscoelasticity of the polymers can violate the foundational elastic contact mechanics. However, the high frequency oscillations appear to minimize the contribution of the viscous component on the measurement of elastic modulus for most elastomeric or glassy polymers.<sup>30</sup> Drzal et al.<sup>6</sup> have recently used nanoindentation to study the effect of UV degradation on the nanomechanical properties of epoxy/TiO<sub>2</sub> nanocomposites. Exposure to UV radiation was found to increase the elastic modulus of top irradiated regions of the nanocomposite, and the rate of increase in the elastic modulus was reduced with increasing volume fraction of nanoparticles. Monney et al.<sup>5</sup> also found that Young's modulus and hardness of two epoxy materials increased with UV irradiation time and continuously decreased with the indentation depth. The formation of a thin photooxidation layer was found at the sample surface due to photodegradation.

In this study, an epoxy/polyurethane (EPO/PU) multilayer system was selected and exposed to the outdoor environment in Gaithersburg, MD, for 6 months. Thickness of the epoxy layer is approximately 300  $\mu\text{m}$  and the polyurethane layer approximately 150  $\mu\text{m}$ . Because of the great thickness for both toplayer and underlayer, it is nearly impossible to have an effective depth profiling using the above instruments without an appropriate sampling. It has been a great success to examine the automotive paint systems as a function of depth since Bohnke et al.<sup>31</sup> invented the in-plane microtomy to study the migration of ultraviolet light absorber (UVA) and hindered amine light stabilizer (HALS) between coating layers. Haacke et al.<sup>32</sup> developed this in-plane microtomy to obtain  $T_g$  and crosslink density profiles and then Adamsons et al.<sup>33</sup> used it to produce chemical depth profiles for the automotive coating systems. Gerlock

and his coworkers<sup>34</sup> also used this technique to acquire the  $\sim 5 \mu\text{m}$  thick slices for their studies on long-term weathering performance of automotive coatings. In the present work, however, cross-sectional microtomy was used to prepare specimens for depth profiling of the mechanical and chemical properties of the EPO/PU multilayer system before and after UV exposure. Compared to in-plane microtomy, cross-sectional sampling is more suitable for a continuous chemical mapping by micro-FTIR imaging and a continuous mechanical profiling by nanoindentation which has sub-micron spatial resolution. To the best of our knowledge, this is the first publication using both micro-FTIR imaging and nanoindentation to probe the spatial distribution of chemical and mechanical properties of a photodegraded multilayer polymeric system. The relationship between the chemical degradation and the mechanical changes during UV exposure is also discussed.

## Experimental<sup>1</sup>

### Specimen preparation

Cross-sectioned specimens were prepared from a model EPO/PU two-layer systems before and after outdoor exposure in Gaithersburg, MD. The epoxy was a non-UV stabilized, unpigmented, stoichiometric mixture of a diglycidyl ether of bisphenol A (DER 332, Dow Chemical) and 1,3-bis(aminomethyl)-cyclohexane (1,3 BAC, Aldrich). The PU was a two-part, black pigmented acrylic urethane (customized by Sherwin-Williams Company) containing 2.5% (based on PU mass) of a UV stabilizer (Tinuvin 1130, Ciba). The PU layer was prepared by casting the UV-stabilized, two-part mixture on release agent-treated aluminum panels by drawdown. Coated samples were cured at room temperature for 24 h, followed by heating at 130°C for 10 min in an air circulating oven. The epoxy/curing agent mixture in solvent was then applied to the partially cured PU film by drawdown in a CO<sub>2</sub>-free, dry glove box to avoid the amine blushing effect.<sup>11</sup> The EPO/PU coated samples were then cured in the glove box at room temperature for 24 h, followed by heating at 130°C for 2 h in an air circulating oven. Thickness of the cured epoxy layer ranged from 280 to 350  $\mu\text{m}$  while the polyurethane layer ranged from 120 to 200  $\mu\text{m}$ . The double-layered EPO/PU free films were removed from the panels and cut into a sample size of approximately 36 x 36 mm<sup>2</sup>. Some samples were used for measuring the initial properties of EPO/PU system, while others were exposed to outdoor environments. Cross-sectional

<sup>1</sup> Certain commercial product or equipment is described in this paper in order to specify adequately the experimental procedure. In no case does such identification imply recommendation or endorsement by the National Institute of Standards and Technology, nor does it imply that it is necessarily the best available for the purpose.

specimens were prepared from both unexposed and exposed systems. For the chemical mapping measured by the FTIR microscope, the approximately 500 nm thick cross-sectioned slices were prepared by a microtome (MT-990, RMS Products). Nanoindentation samples were prepared by embedding the multilayer EPO/PU samples (both UV exposed and unexposed) in a mounting compound, which was composed of 25 parts of an epoxy resin (EPOES, Struers Inc.) and three parts of a hardener (EPOAR, Struers Inc.) by mass fraction. After curing at room temperature for 24 h, the hardened mounted samples were ground and polished, after which nanoindentation measurements were made.

### UV exposure condition

Outdoor UV exposures were carried out in Gaithersburg, MD for 4 months starting from July 2002. Specimens were placed in an environmental chamber at 5° from the horizontal plane facing south (Fig. 1). The bottom of the chamber was made of black-anodized aluminum bottom covered with “borofloat” glass; all four sides of the chamber were covered with a nonmoisture absorbing fabric material, which acted as a filter to prevent dust particles from entering the chamber. UV-visible spectral results showed that the borofloat glass did not alter the solar spectrum before or after more than one-year exposure in Gaithersburg, MD. The chamber was equipped with a thermocouple and a RH sensor, and the temperature and relative humidity in the chamber were recorded continuously.

### Measurement techniques

#### Nanoindentation

Mechanical properties of the embedded cross-sectioned samples were measured using an instrumented nanoindenter (NanoXP, MTS Nanoinstruments, Oak Ridge, TN) and a 1- $\mu\text{m}$  radius 60° diamond conical



Fig. 1: The chamber used for outdoor exposure, showing the exposure cells, the radiometer, and the wires connecting to the temperature and relative humidity sensors

indenter. Depth sensing indentation parameters of 45 Hz and 5 nm amplitude dynamic oscillations were superimposed onto the loading portion of the indentation experiments to determine the contact stiffness. Indenter tip shape has been measured for this probe using indentation of a fused silica reference sample. All indentation experiments were conducted using a strain rate of  $0.05 \text{ s}^{-1}$  and were indented to a depth of about 1.5  $\mu\text{m}$ . A Poisson's ratio of 0.33 was assumed for all polymeric layers and reported values of modulus were averaged over depths from 500 to 1000 nm. The nanoindenter was programmed to perform 50–60 indents while traveling across the thickness of a multilayer sample. A schematic drawing of a molded cross-sectioned sample after nanoindentation is displayed in Fig. 2. The blue marks across interfaces are the residual indents resulting from nanoindentation. Additional details about nanoindentation on multilayer samples can be found in a recent work by Drzal et al.<sup>35</sup>

#### Confocal microscopy

A Zeiss model LSM510 reflection laser scanning confocal microscope (LSCM) was employed to characterize the surface morphology of the multilayer cross section and to measure the distance between indents resulting from nanoindentation testing. A detailed description of LSCM measurements can be found elsewhere.<sup>36</sup> The laser wavelength used in this study was 543 nm. LSCM images are two-dimensional (2D) intensity projections resulting from a series of overlapping optical slices (a stack of z-scan images) with a z-step of 0.1  $\mu\text{m}$ . The 2D intensity projection images are effectively the sum of all the light scattered by

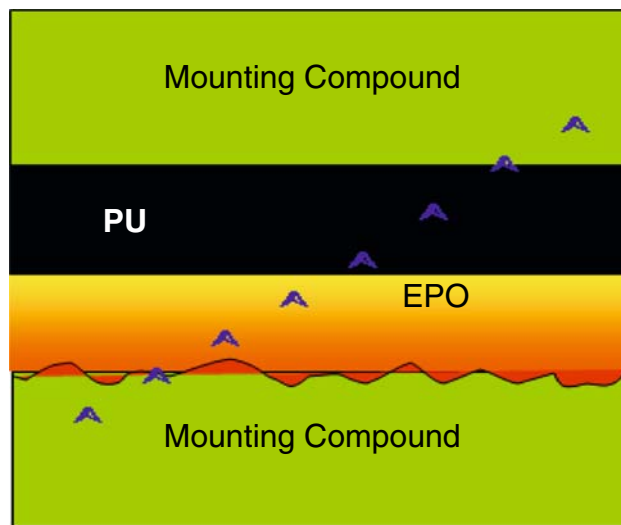


Fig. 2: A schematic drawing of a molded, cross-sectioned EPO/PU multilayer specimen after nanoindentation. Blue marks represent indents

different layers of the coating, limited by the maximum depth of light penetration. The pixel intensity level represents the total amount of back-scattered light. Darker areas represent regions that scatter less light than lighter colored regions do.

### Micro-FTIR imaging

FTIR transmission images were recorded on an imaging microscope equipped with an indium antimonide, 64 pixel x 64 pixel, focal plane array (Digilab Stingray). The samples are illuminated in transmission and the focal plane of the 15×, 0.50 NA Schwarzschild objective is imaged onto the array. The field of view of the microscope is 384 x 384 μm<sup>2</sup>. The IR radiation is directed into the microscope from a Fourier transform IR spectrometer (Digilab FTS-700) equipped with a potassium bromide (KBr) beamsplitter. An interferogram is recorded on each array element, yielding 4096 spectra for each image. The spectra reported here result from the signal averaging of 64 mirror scans, each acquired with an optical retardation velocity of 0.16 cm s<sup>-1</sup>, and nominal resolution of 4 cm<sup>-1</sup> using a triangle apodization function.

## Results and discussion

### Depth profiling of mechanical properties of multilayered samples before and after UV exposure

Figure 3 shows a confocal microscopic image of indentations conducted across the cross section of a molded, unexposed epoxy/polyurethane (EPO/PU) multilayer sample. The rectangle identifies the path of the indents across the sample. The black dots within the rectangle are the residual indents resulting from plastic deformation of the materials after nanoindentation. The interface between the epoxy and the black polyurethane is clearly visible; thus, using the indent at

the EPO/PU interface as the origin, the position of the other indents can be located. Figure 4 is a plot of the elastic modulus as a function of distance from the EPO/PU interface of the same specimen. The assignment of different regions in the plot to the different layers is based on the analysis of the modulus change and the indented marks observed in the confocal image. Two regions on either end of the plot that show a much lower modulus than other regions identify the mounting compound (M). The left side of the EPO/PU interface corresponds to the unexposed epoxy layer, while the right side to the polyurethane layer. A small decrease in modulus is observed in the EPO/PU interface from the epoxy side to the PU side. A constant value, (3.6 ± 0.1) GPa, of the elastic modulus is observed in the epoxy layer, which is consistent with the surface modulus of an unexposed free-standing epoxy film measured directly from the sample surface by nanoindentation. It indicates that the surface and the bulk of the unexposed epoxy have similar modulus values. The PU layer has a slightly lower modulus than the epoxy layer, which is consistent with the results from dynamic mechanical analysis.

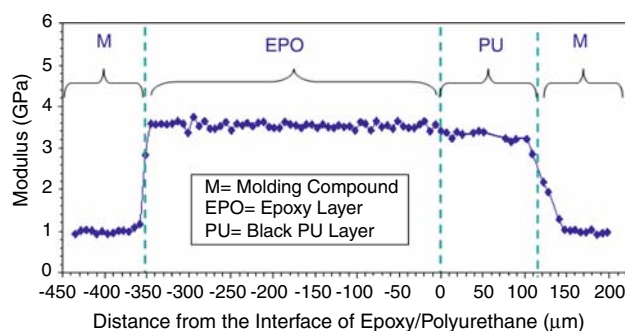


Fig. 4: Elastic modulus as a function of distance from the interface of epoxy/polyurethane for an unexposed epoxy/polyurethane cross-sectioned sample. The average of the modulus in the epoxy layer is (3.6 ± 0.1) GPa. Uncertainties for all data points are less than 5%

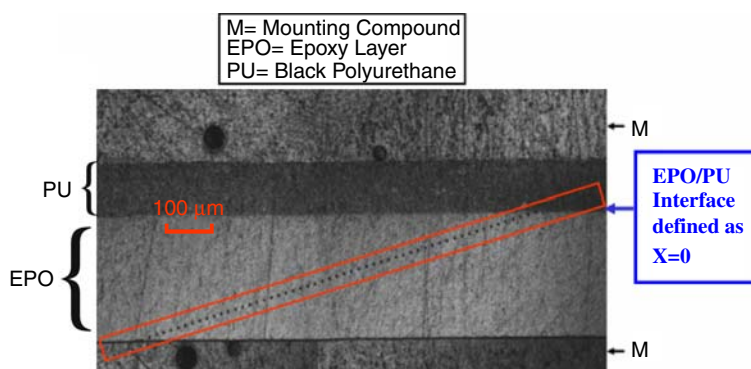


Fig. 3: Confocal microscopic image of the cross section of an unexposed epoxy/polyurethane sample embedded in mounting compound. The rectangle indicates the path of indenter travels across the thickness of the sample

Caution should be exercised when interpreting the modulus results for regions close to an interface having dissimilar properties, as in the case of M/EPO or PU/M. The gradual change of the modulus near the PU/M interface may be an indication of the diffusion of the mounting compound to the PU layer during the preparation of the encapsulated cross-sectioned sample. On the other hand, the sharp increase in the modulus from mounting compound to epoxy layer in the M/EPO interfacial region may suggest that the interdiffusion effect is minimal.

Figure 5 shows the elastic modulus as a function of distance from the EPO/PU interface for an outdoor exposed epoxy/polyurethane cross-sectioned sample. Compared to the data of the unexposed sample (Fig. 4), an obvious increase in the modulus from  $(3.6 \pm 0.1)$  GPa to  $(4.5 \pm 0.1)$  GPa is observed on the surface of the exposed sample. Similar results have been observed in other epoxy systems after UV exposure.<sup>6,14</sup> We believe that this increase is due to the photodegradation of the epoxy through oxidation. The modulus then gradually decreases to a value of  $(3.7 \pm 0.1)$  GPa at some distance from the surface. It remains essentially constant in the interior region of the film but rises rather sharply in the region near the EPO/PU interface. This interesting behavior is discussed further below.

As can be seen in Fig. 5, the modulus value in the plateau is only slightly higher than that of the unexposed epoxy, suggesting that the epoxy in this region probably has not been substantially degraded, at least not dramatically enough to significantly change the modulus. Based on the distance between the surface and the plateau, we suggest that a photodegraded layer with significantly increased modulus has formed in the region about  $62 \mu\text{m}$  deep from the surface into the epoxy bulk.

### Spatial distribution of chemical species in cross-sectioned samples before and after UV exposure

FTIR transmission microscopy was used to image the spatial distribution of chemical species along the

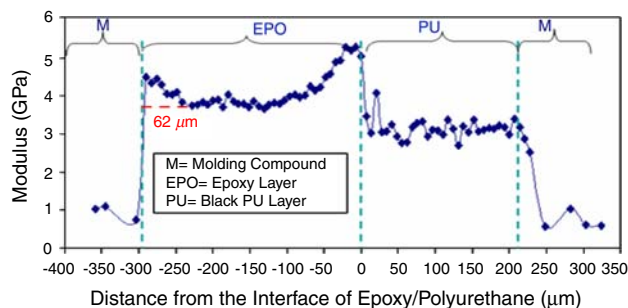


Fig. 5: Elastic modulus as a function of distance from the interface of epoxy/polyurethane for an outdoor exposed epoxy/polyurethane cross-sectioned sample

thickness direction for the cross sections of samples unexposed and exposed to the same outdoor conditions as those for nanoindentation. This technique yields spectral images that contain full IR spectra for each  $6 \times 6 \mu\text{m}^2$  sample region that is imaged onto each array detector pixel ( $64 \times 64$ ). These spectra can be analyzed to generate spatial maps of chemical species based on the area under absorption features due to those species.

Based on analyses of the IR spectra of the unexposed epoxy region (Fig. 6a) and the unexposed polyurethane region (Fig. 6b), both of which were from the cross sections of the fresh EPO/PU sample, and the IR spectrum of the surface region of the outdoor exposed sample (Fig. 6c), chemical maps of three species of interest can be created from the area under three absorption features peaked at 1510, 1693, and  $1658 \text{ cm}^{-1}$ , respectively. The band of  $1510 \text{ cm}^{-1}$ , which is attributed to benzene ring stretching, is a strong and characteristic peak in the epoxy region. Our previous studies<sup>11,13</sup> indicated that during photodegradation, the intensity of  $1510 \text{ cm}^{-1}$  decreased with exposure, and the growth of new absorptions was observed in the region between  $1620$  and  $1800 \text{ cm}^{-1}$ . The broad band around  $1658 \text{ cm}^{-1}$  has been assigned to C=O stretching of an amide<sup>37,38</sup> resulting from photo-oxidation or a quinone methide structure.<sup>39</sup> The band at  $1693 \text{ cm}^{-1}$ , which is attributed to C=O stretching in the urea, is a typical absorption for this selected polyurethane. Since the spectra of epoxy and the polyurethane do not significantly overlap in the regions of these three absorption bands, the areas under 1510, 1693, and  $1658 \text{ cm}^{-1}$  are used for mapping the epoxy region, the polyurethane region and the oxidation products, respectively, for the unexposed and exposed cross-sectioned samples.

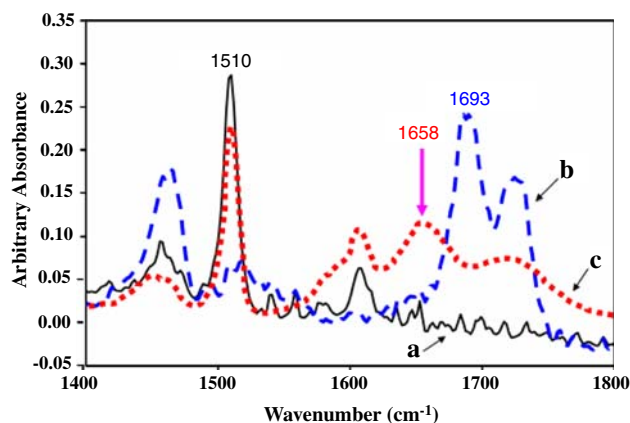


Fig. 6: FTIR spectra in the range between  $1400$  and  $1800 \text{ cm}^{-1}$  of (a) an unexposed epoxy region (solid line), and (b) an unexposed polyurethane region (dashed line), both of which were from the cross sections of the fresh EPO/PU sample, and of (c) a surface region of the outdoor exposed EPO/PU cross-sectioned sample (dotted line)

Figure 7a–c shows the  $384 \times 384 \mu\text{m}^2$  color maps of the epoxy, urethane, and oxidation product species for the exposed sample, respectively. The color scale in Fig. 7a extends from zero (blue) to 9.5 (red) in units of area under the  $1510 \text{ cm}^{-1}$  absorbance band. Note that the width of the effective imaging area of the cross section is only about  $180 \mu\text{m}$  (y-direction) because parts of the sample are out of the microscope focus due to part of the specimen curling. All of the analysis has been done on the brightest region of the sample bounded by the dashed line box as shown in Fig. 7a. The blue area on the left side of the image is air and the yellow solid line marks the approximate position of the air/epoxy interface at the coating surface. The red area of an approximate thickness of  $280 \mu\text{m}$  is the epoxy region of the coating cross section, while the blue region on the right side is due to the polyurethane layer. The position of the epoxy/urethane interface is confirmed by the urethane map in Fig. 7b where the narrow red section on the right identifies the polyurethane region. The approximate epoxy/urethane interface is also marked by a solid yellow line. The color scale in this image extends from zero (blue) to 40.0 (red) in units of area under the  $1693 \text{ cm}^{-1}$  absorbance band. Careful examination of images in Fig. 7 indicate that the air/epoxy and epoxy/urethane interfaces are quite sharp and that the interfacial width is smaller than can be measured with IR microscopy. The apparent interfacial widths in these images are dominated by the instrumental spatial resolution, which is on the order of  $15 \mu\text{m}$  at these imaging wavelengths.

Figure 7c is a color map of the carbonyl containing oxidation products, extending from zero (blue) to 2.0 (red) in units of area under the  $1658 \text{ cm}^{-1}$  absorbance band. The carbonyl map shows an interesting spatial dependence, peaking near the air/epoxy interface (the coating surface), decreasing in the center of epoxy region and increasing again toward the epoxy/urethane interface. This behavior can be seen most clearly in Fig. 8 where the carbonyl stretching band area averaged in the y-direction within the boxed area in Fig. 7a is plotted as a function of the X-axis position in the image. The X-axis position equal to

zero in this plot corresponds to the left edge of the images in Fig. 7. The peak carbonyl intensity around  $80 \mu\text{m}$  corresponds to the red area near the air/epoxy interface in Fig. 7c while the broad peak around  $300 \mu\text{m}$  corresponds to the second bright region in Fig. 7c near the epoxy/urethane interface. The rise in the carbonyl band area near the air/EPO interface is quite slow given that the same interface appears quite sharp in the image in Fig. 7a. This effect is largely due to the averaging over the analysis area. Due to the nonuniform edge of the cross-sectioned sample, the position of air/epoxy interface on the x-axis varies in the analysis region, leading to a blurring of the apparent interfacial width in the average carbonyl band area plot. The negative carbonyl band area in the urethane region has no physical significance and is due to spectral interference between the photooxidation product carbonyl band and the urea carbonyl band.

Similar IR spectral images of EPO/PU cross-section samples before exposure to outdoor environments are

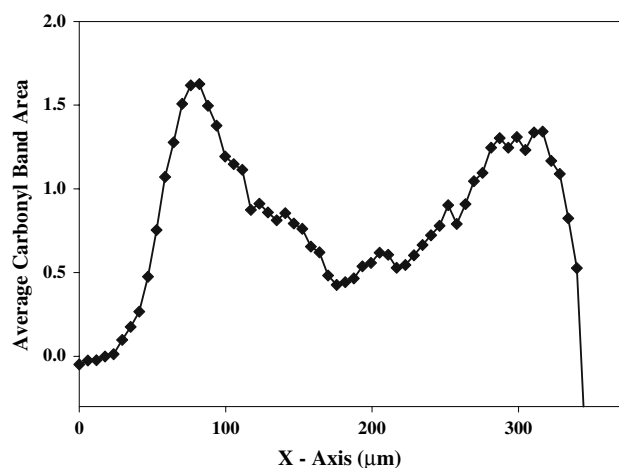


Fig. 8: Plot of the carbonyl band area averaged in the y-dimension within the boxed region shown in Fig. 7a vs the image x-axis. Uncertainties for all data points are less than 10%

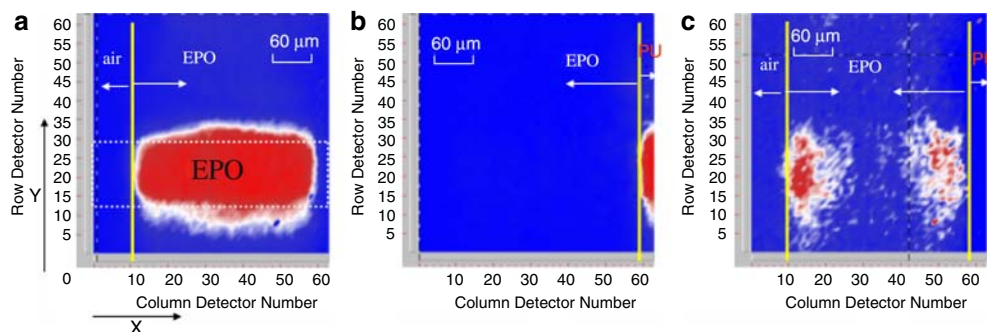


Fig. 7:  $384 \times 384 \mu\text{m}^2$  maps of the area under the (a)  $1510 \text{ cm}^{-1}$  epoxy band, (b)  $1693 \text{ cm}^{-1}$  urethane band, and (c)  $1658 \text{ cm}^{-1}$  photooxidation product band derived from FTIR transmission images of a microtomed cross section of a UV exposed epoxy coating on black pigmented polyurethane (EPO/PU)

shown in Fig. 9. There is no evidence of carbonyl oxidation product formation, with the  $1658\text{ cm}^{-1}$  band areas of nominally 0.1 compared to the peak values of 1.6 seen in Fig. 8 for the exposed samples. This is true for all spatial regions of the unexposed, cross-sectioned sample including areas close to the air/epoxy interface (Fig. 9a, c) and epoxy/urethane interface (Fig. 9b, d). As mentioned previously, the negative values of the carbonyl band area in the PU region shown in Fig. 9d have no physical significance and are due to spectral interference. This observation confirms that the presence of carbonyl containing compounds is due to degradation of epoxy materials during outdoor exposure.

Comparing the micro-IR profiles of the exposed sample with the depth profiling from nanoindentation, one can find that the spatial distribution of the oxidized products with absorptions around  $1658\text{ cm}^{-1}$  has similar trend as the modulus profile as a function of depth (Figs. 5, 7c, 8). Both the concentration of oxidized products and the modulus value summit near the degraded coating surface, decreasing in the center of epoxy region and increasing again toward the epoxy/urethane interface. The region with significant amounts of photoproducts just beneath the surface (red colored region in Fig. 7c) corresponds to the region with the pronounced modulus increase, both of which are approximately  $60\text{ }\mu\text{m}$  deep from the sample surface.

This consistency indicates that the modulus increase of the degraded region may be related to the formation of the oxidized products, even though the internal stress in the interface could play a role as well. Mailhot et al.<sup>14,16</sup> have attributed the increase of the stiffness in the photodegraded polymers to the predominance of crosslinking, while the decrease in stiffness mainly to chain scission. In our case, further studies need to be done to clarify the degradation mechanism of the studied epoxy because our dynamic mechanical analysis has shown that the glass transition temperature of the epoxy bulk decreases with the longer outdoor exposure.

Careful examination of the chemical and mechanical depth profiles reveals further information about the relationship between the chemical degradation and the mechanical changes resulting from photodegradation. As can be seen in Fig. 5, the interior epoxy region with relatively constant modulus is much wider than the epoxy region with low carbonyl concentration of oxidized products (the valley in Fig. 8). Since the modulus in the interior epoxy region is only slightly higher than that of the unexposed epoxy, the above difference between the chemical spatial distribution and the mechanical property spatial variation indicates that the chemical changes may take place earlier than the visible mechanical changes. This suggests that significant amounts of oxidized products are required

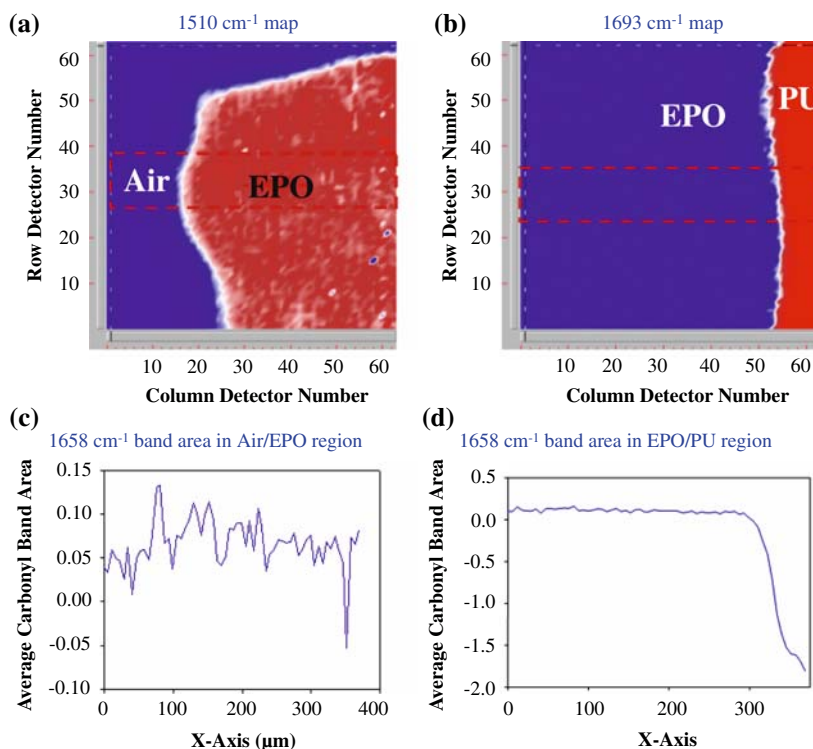


**Fig. 9:**  $384 \times 384\text{ }\mu\text{m}^2$  maps of the area under the (a)  $1510\text{ cm}^{-1}$  epoxy band, (b)  $1693\text{ cm}^{-1}$  urethane band of a microtomed cross section of an unexposed epoxy coating on black pigmented polyurethane (EPO/PU); (c) and (d) are the plots of band areas in the carbonyl region ( $1658\text{ cm}^{-1}$ ) averaged in the y-dimension within the boxed region shown in (a) and (b) vs the image x-axis. Uncertainties for all data points are less than 10%

to bring about the obvious increase in the modulus. However, this conclusion is based on the current research; the ability to sense chemical and mechanical changes may be system dependent.

The observed heterogeneous distribution of the chemical species and the mechanical properties could be explained by two factors: the light penetration and the oxygen permeability.<sup>14,40</sup> The peak in the oxidation products near the air/epoxy interface is consistent with expectations for a photooxidation process driven by UV exposure, wherein the subsequent decay in carbonyl products with increasing depth into the epoxy reflects the decrease in the number of photons absorbed at that depth. The UV–visible spectra of the epoxy films (not shown) indicate that the epoxy topcoat has an approximately 50% of UV absorbance at 340 nm. As exposure proceeds, the attenuation of UV light from the epoxy layer is becoming more severe due to the formation of the chromophoric photoproducts through epoxy degradation.<sup>16</sup> The transmission of 340 nm UV radiation to the underlying PU layer is only about 5% after 1 month outdoor exposure. The more surprising result is the peak in carbonyl containing products in the epoxy region near the epoxy–urethane interface, where a sharp increase in the modulus is also observed. The reason for the high concentration of carbonyl products in this region is not certain, while several mechanisms are possible. The interdiffusion and reaction of epoxy and polyurethane in the interface might yield a carbonyl formation. However, no evidence of such diffusion and reaction has been found because the EPO/PU interface is quite sharp for both exposed and unexposed samples, as shown in Figs. 7 and 9. Another possibility for the carbonyl formation is due to the photooxidation in the EPO/PU interfacial region. Similar results have been reported by Gerlock et al.<sup>34</sup> in their studies on weathering performance of multilayer automotive paint systems. Because of the limited UV screening effect from epoxy toplayer, the EPO/PU interfacial region and the PU underlayer can be photoliable. Compared to the interior of epoxy layer, the EPO/PU interfacial region would have a relatively higher temperature, which results from the light absorption in the black PU, and a preferential oxygen accessibility because the interface is susceptible to delamination as a consequence of the hygrothermal stresses during outdoor exposure. These two factors are both favorable to the oxidized product formation and the related modulus increase in the EPO/PU interfacial region, rather than within the epoxy interior. However, further studies need to be done to investigate if these factors are the main aspects to cause the differences between the epoxy interior and the interfacial region. Nevertheless, the changes of the depth profiles of chemical and mechanical properties of this EPO/PU system suggest that, not only the topcoat, but also the topcoat/basecoat interfacial region of a multilayer sample can be subjected to photodegradation during outdoor exposure. The photodegradation in this region may

lead the topcoat/basecoat interface to be the most susceptible region to the outdoor weathering conditions in the multilayer system.

## Summary

Depth profiling mechanical and chemical changes of an epoxy/polyurethane multilayer polymeric system has been investigated by nanoindentation and micro-FTIR imaging using cross-sectioned samples. Significant amounts of oxidation products are observed in the 60  $\mu\text{m}$  deep region from the degraded surface to the epoxy bulk, and then the concentration of carbonyl products subsequent decreases with increasing depth into the epoxy. Nanoindentation results also show that the modulus significantly increases in the first 60  $\mu\text{m}$  region after UV degradation, and then decreases gradually with depth until a value slightly higher than the modulus of the undegraded epoxy is reached. The presence of carbonyl containing products also increases near the EPO/PU interface along with the increase in the modulus. The reason for this change is not certain. One possibility could be due to the photooxidation in the EPO/PU interfacial region. This study clearly shows that the spatial distribution of chemical species and the mechanical properties is heterogeneous in thickness direction for polymer coatings after UV degradation. The shapes of the chemical depth profile (oxidized products) and the spatial variation in the mechanical properties are similar but not exactly the same. It suggests that the modulus increase of the degraded region may be related to the oxidized products formation. However, significant amounts of oxidized products are required to bring about an obvious increase in the modulus. This study also demonstrates that cross-sectional analysis using nanoindentation and micro-FTIR imaging techniques is a useful method to characterize the mechanical and chemical depth profiles of polymer coating degradation.

**Acknowledgments** This research is part of a Government/Industry consortium on Service Life Prediction of Coatings at NIST. Companies involved in this consortium include Akzo Nobel, Arkema Inc., Atlas Material Testing Technologies LLC, Dow Chemical, and Sherwin Williams. Federal Highway Administration, Wright Patterson AFB, and Forest Products Laboratory also provided additional funds for this research. We thank Dow Chemical for providing the epoxy resin, and Sherwin Williams for providing the urethane resin.

## References

1. Rabek, JF, *Polymer Photodegradation—Mechanisms and Experimental Methods*, pp. 269–278. Chapman & Hall, New York (1995)
2. Hill, DJT, Le, TT, O'Donnell, JH, Perera, MCS, Pomery, PJ, In: Reichmanis, E, Frank, CW, O'Donnell, JH (eds.)

- Irradiation of Polymeric Materials: Processed, Mechanisms, and Applications.* American Chemical Society, Washington (1993)
3. Hill, LW, Korzeniowski, HM, Ojungaandrew, M, Wilson, RC, "Accelerated Clearcoat Weathering Studied by Dynamic-Mechanical Analysis." *Prog. Org. Coat.*, **24** (1–4) 147 (1994)
  4. Hill, LW, Grande, JS, Kozlowski, K, "Dynamic Mechanical Analysis of Weathered (Q-U-V(R)) Acrylic Clearcoats With and Without Stabilizers." *Proc. ACS Div. Polym. Mater. Sci. Eng.*, **63** 654 (1990)
  5. Delobelle, P, Guilot, L, Dubois, C, Monney, L, "Photo-Oxidation Effects on Mechanical Properties of Epoxy Matrixes: Young's Modulus and Hardness Analyses by Nanoindentation." *Polym. Degrad. Stab.*, **77** 465 (2002)
  6. Drzal, PL, Scierka, S, Forster, AL, Svetlik, S, "Effects of UV Degradation on the Nanomechanical Properties of TiO<sub>2</sub>/Epoxy Nanocomposites." *Proc. 28th Annual Meeting of the Adhesion Society*, 2005, p. 524
  7. Faucheu, J, Wood, KA, Sung, LP, Martin, JW, "Relating Gloss Loss to Topographical Features of A PVDF Coating." *J. Coat. Technol. Res.*, **3** (1) 29–39 (2006)
  8. Hunt, FY, Galler, MA, Martin, JW, "Microstructure of Weathered Paint and its Relation to Gloss Loss: Computer Simulation and Modeling." *J. Coat. Technol.*, **70** (980) 45–54 (1998)
  9. Nguyen, T, Martin, J, Byrd, E, "Relating Laboratory and Outdoor Exposure of Coatings: IV. Mode and Mechanism For Hydrolytic Degradation of Acrylic-Melamine Coatings Exposed to Water Vapor in The Absence of UV Light." *J. Coat. Technol.*, **75** (941) 37–50 (2003)
  10. Van Landingham, MR, Nguyen, T, Byrd, WE, Martin, JW, "On the Use of the Atomic Force Microscope to Monitor Physical Degradation of Polymeric Coating Surfaces." *J. Coat. Technol.*, **73** (923) 43–50 (2001)
  11. Gu, X, Nguyen, T, Oudina, M, Martin, D, Kidah, B, Jasmin, J, Rezig, A, Sung, L, Byrd, E, Martin, JW, "Microstructure and Morphology of Amine-Cured Epoxy Coatings Before and After Outdoor Exposures—An AFM Study." *J. Coat. Technol. Res.*, **2** (7) 547–556 (2005)
  12. Gu, X, Nguyen, T, Sung, L, VanLandingham, MR, Fasolka, MJ, Martin, JW, Jean, YC, Nguyen, D, Chang, NK, Wu, TY, "Advanced Techniques For Nanocharacterization of Polymeric Coating Surfaces." *J. Coat. Technol. Res.*, **1** (3) 191–200 (2004)
  13. Rezig, A, Nguyen, T, Martin, D, Sung, L, Gu, X, Jasmin, J, Martin, JW, "Relationship Between Chemical Degradation And Thickness Loss of An Amine-Cured Epoxy Coating Exposed to Different UV Environments." *J. Coat. Technol. Res.*, **3** (3) 173–184 (2006)
  14. Mailhot, B, Bussiere, P-O, Rivaton, A, Morlat-Therias, S, Gardette, J-L, "Depth Profiling by AFM Nanoindentations and Micro-FTIR Spectroscopy for the Study of Polymer Ageing." *Macromol. Rapid Commun.*, **25** 436 (2004)
  15. Bokria, JG, Schlick, S, "Spatial Effects in the Photodegradation of Poly(acrylonitrile-butadiene-styrene): A Study by ATR-FTIR." *Polymer*, **43** 3239 (2002)
  16. Mailhot, B, Morlat-Therias, S, Bussiere, P-O, Gardette, J-L, "Study of the Degradation of an Epoxy/amine Resin, 2 Kinetics and Depth-Profiles." *Macromol. Chem. Phys.*, **206** 85 (2005)
  17. Gonon, L, Mallegol, J, Commereuc, S, Verney, V, "Step-Scan FTIR and Photoacoustic Detection to Assess Depth Profile of Photooxidized Polymer." *Vibrat. Spectrosc.*, **26** 43 (2001)
  18. Katti, KS, Urban, MW, "Conductivity Model and Photoacoustic FT-IR Surface Depth Profiling of Heterogeneous Polymers." *Polymer*, **44** 3319 (2003)
  19. Dittmar, RM, Chao, JL, Palmer, R, *Springer Series in Optical Science: Photoacoustic and Photothermal Phenomena III*, Vol. 6, p. 492. Springer, Berlin (1992)
  20. Jouan, X, Gardette, JL, "Development of A Micro (FTIR) Spectrophotometric Method For Characterization of Heterogeneities in Polymer-Films." *Polym. Commun.*, **28** 329 (1987)
  21. Mailhot, B, Gardette, J-L, "Polystyrene Photooxidation .2. A Pseudo Wavelength Effect." *Macromolecules*, **25** 4127 (1992)
  22. Rivaton, A, Moreau, L, Gardette, J-L, "Photo-Oxidation of Phenoxy Resins at Long and Short Wavelengths—I. Identification of the Photoproducts." *Polym. Degrad. Stab.*, **58** 321 (1997)
  23. Rivaton, A, Mailhot, B, Soulestin, J, Varghese, H, Gardette, J-L, "Influence of the Chemical Structure of Polycarbonates on the Contribution of Crosslinking and Chain Scissions to the Photothermal Ageing." *Eur. Polym. J.*, **38** 1349 (2002)
  24. Gonon, L, Vasseur, OJ, Gardette, J-L, "Depth Profiling of Photooxidized Styrene-Isoprene Copolymers by Photoacoustic and Micro-Fourier Transform Infrared Spectroscopy." *Appl. Spectrosc.*, **53** 157 (1999)
  25. VanLandingham, MR, Villarrubia, JS, Guthrie, WF, Meyers, GF, "Nanoindentation of Polymers: An Overview." *Macromol. Symp.*, **167** 15 (2001)
  26. Oliver, WC, Pharr, GM, "Measurement of Hardness and Elastic Modulus by Instrumented Indentation: Advances in Understanding and Refinements to Methodology." *J. Mater. Res.*, **19** 3 (2004)
  27. Oliver, WC, Pharr, GM, "Measurement of Thin-Film Mechanical-Properties Using Nanoindentation." *J. Mater. Res.*, **7** 1564 (1992)
  28. VanLandingham, MR, "Review of Instrumented Indentation." *J. Res. NIST*, **108** 249 (2003)
  29. VanLandingham, MR, Chang, N-K, Drzal, PL, White, CC, Chang, S-H, "Viscoelastic Characterization of Polymers Using Instrumented Indentation. I. Quasi-Static Testing." *J. Polym. Sci. Part B Polym. Phys.*, **43** 1794 (2005)
  30. White, CC, VanLandingham, MR, Drzal, PL, Chang, N-K, Chang, S-H, "Viscoelastic Characterization of Polymers Using Instrumented Indentation. II. Dynamic Testing." *J. Polym. Sci. Part B Polym. Phys.*, **43** 1812 (2005)
  31. Bohnke, H, Avar, L, Hess, E, "Analytical Studies of Light Stabilizers in Two-Coat Automotive Finishes." *J. Coat. Technol.*, **63** (799) 53 (1991)
  32. Haacke, G, Brinen, JS, Larkin, PJ, "Depth Profiling of Acrylic/Melamine Formaldehyde Coatings." *J. Coat. Technol.*, **67** (843) 29 (1995)
  33. Adamsons, K, Litty, L, Lloyd, K, Stika, K, Swartzfager, D, Walls, D, Wood, B, In: Bauer, DR, Martin, JW (eds.) *Service Life Prediction of Organic Coatings: A Systems Approach*, pp. 257–287. ACS Symposium Series, Vol. 722. Oxford University Press (1999)
  34. Gerlock, JL, Kucherov, AV, Nichols, ME, "On the Combined Use of UVA, HALS, Photooxidation, and Fracture Energy Measurements to Anticipate the Long-term Weathering Performance of Clearcoat/Basecoat Automotive Paint Systems." *J. Coat. Technol.*, **73** (918) 45–54 (2001)
  35. Drzal, PL, Sung, L, Britz, D, Ryntz, R, "Nanomechanical Properties of Polymeric Coatings Through Instrumented Indentation." *Proc. International Coatings for Plastics Symposium*, 2005

36. Sung, LP, Jasmin, J, Gu, X, Nguyen, T, Martin, JW, “Use of Laser Scanning Confocal Microscopy for Characterizing Changes in Film Thickness and Local Surface Morphology of UV-Exposed Polymer Coatings.” *J. Coat. Technol. Res.*, **1** (4) 267–276 (2004)
37. Bellinger, V, Bouchard, C, Claveirolle, P, Verdu, J, “Photo-Oxidation of Epoxy Resins Cured by Non-Aromatic Amines.” *Polym. Photochem.*, **1** 69 (1981)
38. Bellinger, V, Verdu, J, “Oxidative Skeleton Breaking in Epoxy-Amine Networks.” *J. Appl. Polym. Sci.*, **30** 363 (1985)
39. Mailhot, B, Morlat-Therias, S, Ouahioube, M, Gardette, J-L, “Study of the Degradation of an Epoxy/amine Resin, 1.” *Macromol. Chem. Phys.*, **206** 575 (2005)
40. Gillen, KT, Clough, RL, “Quantitative Confirmation of Simple Theoretical-Models for Diffusion-Limited Oxidation.” *ACS Symp. Ser.*, **475** 457 (1991)